Available online at www.sciencedirect.com

ScienceDirect

Procedia CIRP 143 (2026) 722–727

www.elsevier.com/locate/procedia

14th CIRP Conference on Photonic Technologies

Investigation of Powder Catchment Efficiency in Laser-Based Directed Energy Deposition via CFD Modeling and Acoustic Emission

Erik Haapa[a], Mojtaba M. Beidokhti[a], Kandice S. B. Ribeiro[a,*]

[a]Department of Mechanical and Materials Engineering, University of Turku, Turku, FI-20014, Finland

- Invited Paper -

* Corresponding author. *E-mail address:* ksbari@utu.fi

Abstract

Laser-based powder directed energy deposition (DED-LB/P) relies on powder delivery dynamics, which affect process efficiency and part quality through material catchment at the melt pool. This study investigates powder flow behavior and particle catchment using a combined computational and experimental approach. Computational fluid dynamics (CFD) models were developed to simulate material-laser interaction, and powder flow, including particle impact frequency. Model predictions were validated through single-bead deposition of stainless steel 316L powder, monitored using acoustic emission (AE). Simulations provided insight into the frequency of free-powder particle impacts, supporting analysis of powder-substrate interactions. Results show that structure-borne AE signals are sensitive to variations in powder mass flow rate, enabling reliable detection of flow fluctuations. However, direct quantification of powder catchment efficiency from AE remains challenging. The integration of AE monitoring with computational modeling offers a promising pathway for improved understanding and real-time evaluation of powder delivery efficiency and process stability in DED-LB/P.

Keywords: DED-LB; Computational Fluid Dynamics modeling; Catchment efficiency; Process monitoring; Acoustic emission.

1. Introduction

Laser-based Directed Energy Deposition (DED-LB) is increasingly used for manufacturing and repair of high-value metal components due to its high deposition rates and capability for multi-material processing [1]. Typical industrial applications include the repair of turbine blades and shafts tooling components [2], and addition of features to existing parts [3]. Despite these advantages, broader industrial adoption remains limited by challenges related to process stability, variability in bead geometry, and efficiency of feedstock systems [4].

In powder DED-LB systems, only a fraction of the delivered powder is captured by the melt pool and fused into the deposited track [5]. While powder feedstock provides high material flexibility, it generally exhibits lower deposition efficiency and higher cost compared to wire-based systems [4, 6]. Low catchment efficiency increases production costs due to material waste and may also contribute to process instability, irregular bead geometry, and contamination caused by overspray particles [7]. Therefore, understanding powder flow dynamics and particle-melt pool interactions is essential for improving deposition quality and process efficiency.

10.1016/j.procir.2026.07.150

Several sensing approaches have been explored for in-situ monitoring of laser-based additive manufacturing processes. Melt-pool and high-speed imaging are commonly used to observe thermal behavior and track morphology during deposition [8]. To address these complexities, computational fluid dynamics (CFD) has emerged as a critical tool for decoupling the transient physical phenomena occurring within the deposition zone. High-fidelity simulations allow for the precise tracking of particle trajectories that is otherwise hard to observe experimentally. By modeling the interaction between the laser beam, the shielding gas flow, and the powder stream, CFD provides a predictive framework to optimize nozzle designs and process parameters for maximum catchment [9]. Previous CFD studies in DED have primarily focused on the thermo-capillary flow within the melt pool [10]. However, there is a significant lack of research that integrates the discrete powder flow perspective into these models. Most existing simulations treat the powder as a homogenized mass flow or a simplified heat source [9, 10], failing to capture the stochastic nature of individual particle impacts and their contribution to the structural response of the substrate [11]. Bridging this gap requires a multifaceted approach where high-fidelity simulations are validated by high-resolution experimental sensing, e.g. acoustic emission (AE).

While airborne AE microphones can detect melt-pool instabilities causes defect formation in PBF [12], their efficacy in DED is hindered by the shielding gas noises. High-frequency acoustic signals undergo severe atmospheric attenuation, often exceeding 20 dB/cm at frequencies above 100 kHz [13]. In contrast, structure-borne AE sensors mounted directly to the substrate offer a high-fidelity alternative. By capturing elastic waves propagating through the solid medium, these sensors can detect sub-MHz frequencies with minimal signal loss [11]. Although previous laser cladding research has identified specific resonances near 200 kHz associated with particle impacts [14], the quantitative relationship between AE spectral characteristics and key DED-LB parameters, such as powder mass flow rate and laser power, remains largely unexplored.

This study addresses this gap by integrating a thermo-fluid CFD model with structure-borne AE monitoring to investigate the powder flow behavior of AISI 316L. By correlating simulated particle-laser interactions with experimental AE signatures and bead geometries, we establish a predictive framework for real-time assessment of powder catchment efficiency and process stability.

2. Methodology

This study investigates particle impact frequencies during DED-LB, which could be used to assess the powder catchment efficiency and mass flow rate by acoustic emission monitoring. This is done by computational modeling of both the melt pool geometry and the flow of gas and powder from the DED-LB nozzle. Additionally, single DED-LB beads are deposited in practical experiments to enable comparison to the simulations.

2.1. Numerical modeling

Numerical models of the melt pool and the powder delivery system (i.e., DED-LB nozzle) were created using FLOW-3D AM 2025R1 commercial CFD software. The simulation approach consists of two coupled models: (i) a laser-material interaction model to obtain realistic melt pool dimensions for a given catchment efficiency, and (ii) a coupled particle-fluid simulation of the DED-LB nozzle to determine the resulting catchment efficiency and particle impact frequencies, using the melt pool geometry from (i). Both models were applied to two operating conditions representative of lower and upper bounds of experimentally investigated powder mass flow rates of 5.21 and 11 g/min. The models were validated by comparison to experimentally determined deposited bead width and catchment efficiency.

A thermo-fluid simulation of the deposition process was conducted in FLOW-3D AM to obtain the steady-state melt pool shape, as represented in Fig. 1.

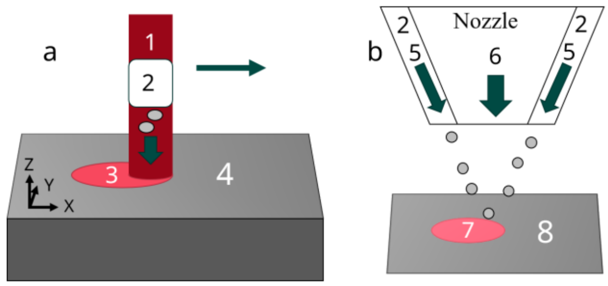

Fig. 1. Setup of the (a) Melt pool simulation (b) Nozzle simulation. 1: Laser beam, 2: Particle generator, 3: Melt pool, 4: 316L substrate, 5: Carrier gas source, 6: Nozzle gas source, 7: Particle counter with melt pool geometry, 8: Particle counter with substrate geometry.

In this first model, the ray-traced laser heat source and powder particle source were translated across the substrate in a straight 16 mm line for 1 second until a steady melt pool geometry was achieved. As shown in Fig. 1, a particle source coupled to the laser beam ejected powder particles directly into the melt pool with initial velocity of 600 mm/s at a generation rate corresponding to the powder catchment efficiency of the physical system. The melt pool simulation considered temperature-dependent thermophysical properties for 316L stainless steel and accounted for key physical mechanisms governing melt pool dynamics, including ray-traced Fresnel reflections of the heat source, surface tension gradient driven flows, and evaporation-induced recoil pressure. The surrounding gas was approximated as a void region with fixed atmospheric pressure and emissive and convective heat transfer boundary conditions on free surfaces. Powder entering the melt pool was modeled as particles which convert into liquid 316L when liquidus temperature is reached, and do not consider particle-particle interactions. The numerical mesh in the laser-material interaction area used a cubic cell size of 0.2 mm, while 0.4 mm cells were used in heat conduction regions 4 mm away from the laser toolpath. The steady-state melt pool geometry obtained from this model was then used to define the melt pool measurement surface in the nozzle simulation, enabling estimation of particle impact frequency and catchment for the investigated parameters.

The second model was created to evaluate the powder delivery and gas flow within the coaxial nozzle, simulated using a CFD model coupled with Discrete Element Method (DEM) particle model. Due to geometric symmetry, only half of the nozzle geometry was modeled to reduce computational cost. The gas was considered as Argon in single-phase turbulent flow using the renormalized group (RNG) k-ε turbulence model. The DEM model considers forces and torques resulting from collision and friction in particle-particle and particle-wall interaction. The particle-fluid (gas) interaction is considered with a two-way coupling scheme. The computational mesh in the nozzle and particle interaction areas used a uniform grid with cubic cell size of 0.2 mm, while gas outflow is handled with progressively coarser 0.4 mm and 0.8 mm grids. A zero normal velocity and zero gradient boundary condition was applied along the central symmetry plane, while other boundaries allowed outflow of gas and particles.

To quantify particle impacts, two measurement surfaces were defined at the substrate level beneath the nozzle, as shown in Fig. 1. The first surface, referred to as the substrate, counted particles that missed the melt pool and impacted the substrate. The second surface, referred to as the melt pool, recorded particles reaching the melt pool region. These surfaces allowed estimation of both particle impact frequency and powder catchment efficiency. To relate the simulated particle impacts to the experimentally observed acoustic emission activity, the particle impact frequency (f_{imp}) can be estimated as in Eq. 1.

$$f_{imp} = N_{imp}/t_{sim} \quad (1)$$

Where N_{imp} represents the number of particles counted at the measurement surface (either substrate or melt pool) and t_{sim} is the simulated physical time. This formulation provides an estimate of the particle impact rate at the substrate or melt pool region.

The simulated free particle impact frequency was calculated based on the same input parameters as in the experimental setup and later correlated with the band-integrated acoustic emission intensity obtained from the Power Spectral Density (PSD) analysis, depicted in the subsection 2.2.

2.2. Experimental setup

The experimental phase of this study was performed on a laser-based Directed Energy Deposition (DED-LB) system mounted on a Yaskawa Motoman six-axis industrial robot. The energy source was a continuous-wave IPG YLS-10000 multimode fiber laser with a maximum output power of 10 kW and a wavelength of 1070 nm. The laser beam was delivered through a 200 µm optical fiber to a Precitec YC52 cladding head with a 300 mm focal length lens. This optical configuration produced a top-hat beam profile expanded to a spot diameter of 1.1 mm.

For model validation, single beads of gas-atomized AISI 316L stainless steel powder (Sandvik Osprey Ltd., Batch 24D0346) with particle sizes ranging from 45 to 106 µm were deposited at and mass flow rate of 11 g/min. To study the relationship of AE signal and simulated catchment, the AE data of an earlier single bead experiment with 5.21 g/min mass flow rate but otherwise same parameters were utilized. In both experiments, the laser power was 1.4 kW and scan speed 16 mm/s, the nozzle featured a cone gap of 0.5 mm and was operated at a standoff distance of 18 ± 0.2 mm from the substrate surface. Argon was used as carrier gas at a flow rate of 5 L/min to transport the powder from the powder feeding system (GTV PF2/2) to the deposition head, while an additional shielding gas flow of 5 L/min was supplied to protect the melt pool from oxidation.

A QASS QWT-series piezoelectric AE sensor was mounted beneath the substrate, which consisted in 8 mm thickness 300x200 mild steel plate, to capture transient elastic waves generated during the process, as shown in Fig. 2.

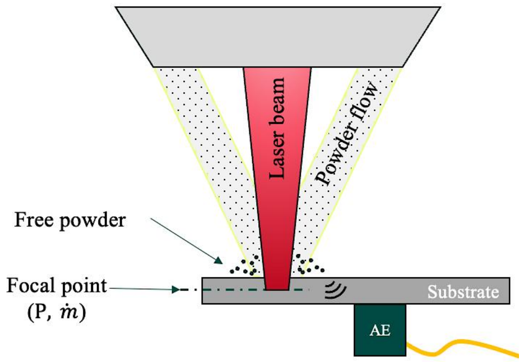

Fig. 2. Schematics of the experimental setup.

According to Buttle et. al. [15], upon the impact of a hard projectile against a massive target, kinetic energy is partitioned into plastic deformation at the contact site, elastic wave propagation, and the residual kinetic energy of the rebounding particle. Research indicates that the energy fraction dissipated as elastic waves is relatively small. For steel spheres impacting a mild steel surface at 70 m/s, only 3 % of the initial energy is converted into acoustic emissions. This acoustic energy is primarily distributed among Rayleigh waves (approximately 67 %), longitudinal waves (5-10 %), and shear waves. These waves propagate through the target according to the elastic properties of the medium, enabling detection by surface-mounted sensors [15]. The Shear mode and the Longitudinal mode are thickness dependent and can be calculated from the Eq. 2 [16]:

$$f_n = nc/2h \quad (2)$$

Where f_n is the frequency in order of $n \geq 1$, c is the velocity of the wave in shear or longitudinal mode in the medium, and h is the thickness of the substrate.

Taking the thickness resonance model presented in Eq. 2, the first order of shear mode (f_S) and longitudinal mode (f_L) for this setup are 200 kHz and 369 kHz, respectively. Frequencies above 900 kHz, associated with shear modes ($n \geq 5$) and longitudinal modes ($n \geq 3$), were not investigated in this study, as the AE sensor's response in the current setup is limited to 1 MHz and cannot reliably measure them. To analyze AE response across the experimental matrix, a workflow based on PSD analysis was implemented. AE signals were segmented according to the process, and PSD estimates were obtained by averaging squared spectral magnitudes and normalizing by bandwidth. A baseline PSD derived from stationary powder-only recordings was subtracted from each active run to isolate process-related emissions. The resulting spectra was integrated over the frequency band of 50-300 kHz to obtain band-intensity features for each phase and condition.

After printing, the bead surfaces were evaluated by an optical 3D microscope model Alicona infinite focus manufactured by Bruker. The dimensions of the beads and the printing volume were used as input for the proposed numerical model. Based on these inputs, the theoretical catchment efficiency was defined as the ratio of resulting bead mass and the mass delivered during process.

3. Results and discussion

Figure 3 presents the proposed melt pool and nozzle simulation plots. The simulated melt pool for the tested conditions was elongated, with semicircular leading edge and elliptical trailing edges, as shown in Fig. 3, together with the melt pool geometry with the nozzle simulation.

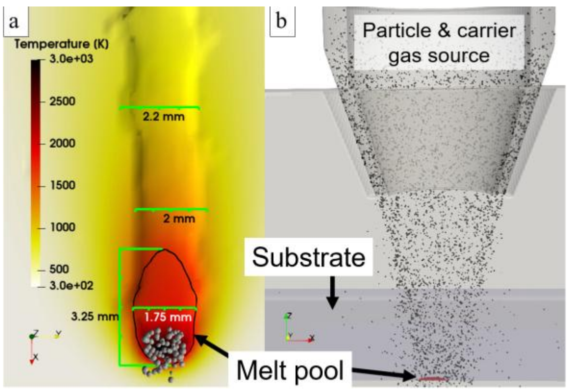

Fig. 3. Simulation of (a) single bead deposition, and (b) powder and gas flow in the nozzle, both with 11 g/min. Particles are scaled 2x for visibility.

The melt pool length for the 11 g/min process was 3.25 mm and 3 mm for 5.21 g/min, and the width of 1.75 mm, approximately, for both processes. To validate the deposition model, bead width was measured from the 11 g/min validation experiment (see Fig. 4).

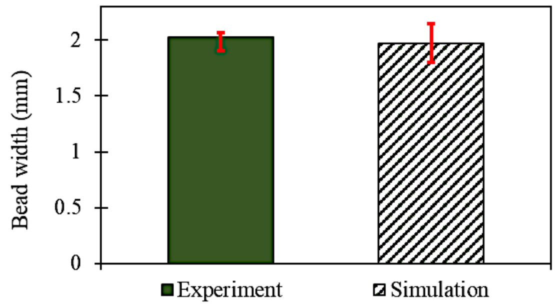

Fig. 4. Melt pool width from experimental and simulated bead deposition with 1.4 kW laser power, 16 mm/s scan speed, and 11 g/min mass flow rate.

The nozzle simulations also show variation in behavior with mass flow rate. At the lower mass flow rate of 5.21 g/min, the particle stream is less focused compared to 11 g/min as seen in Fig. 5. The reason may be that some particles diverge from the main powder stream in both processes, but their proportional share is greater in the low mass flow rate.

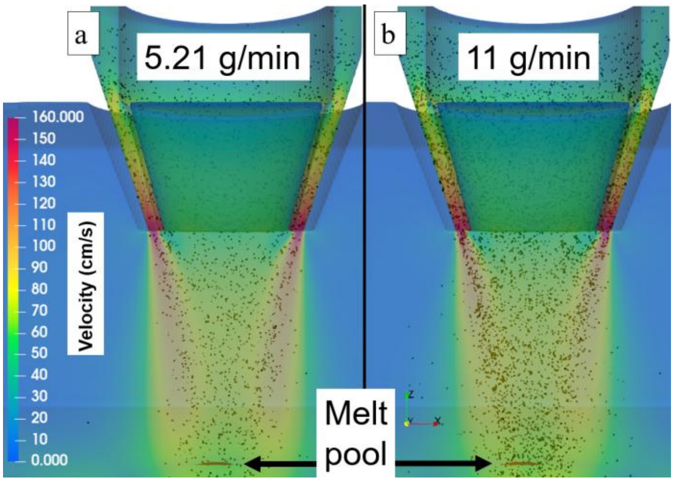

Fig. 5. Particles scaled 2x and gas velocity at (a) 5.21 g/min and (b) 11 g/min.

Combined with the slightly smaller melt pool size, this resulted in lower catchment efficiency as can be seen in Fig. 6, showing that at 11 g/min the simulated average efficiency is 14.5 %, closely matching the experimental results. The 5.21 g/min results however show an inverse trend compared to experimental. The simulation models assume identical initial gas and particle velocity at the top of the nozzle geometry in Fig. 5, while in real experiments it is likely that the velocity of gas depends on the volume of particles carried, affecting the particle stream focus. Additionally, since the number of particles is much lower, the simulated catchment in 5.21 g/min model is more sensitive, and the approximated initial conditions cause divergence from experimental which is not seen in the less sensitive 11 g/min. Further, the 11 g/min experiment was conducted months before the 5.21 g/min, which can affect experiment conditions, e.g., increased moisture in the powder. Together, these factors reduce catchment for experimental 11 g/min and simulated 5.21 g/min.

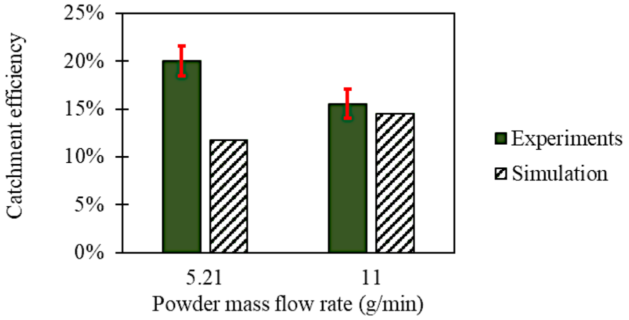

Fig. 6. Computational and experimental powder catchment efficiency at the melt pool for 5.21 and 11 g/min mass flow rates.

The simulated catchment and frequency of particles missing the melt pool and impacting the substrate is presented in Fig. 7.

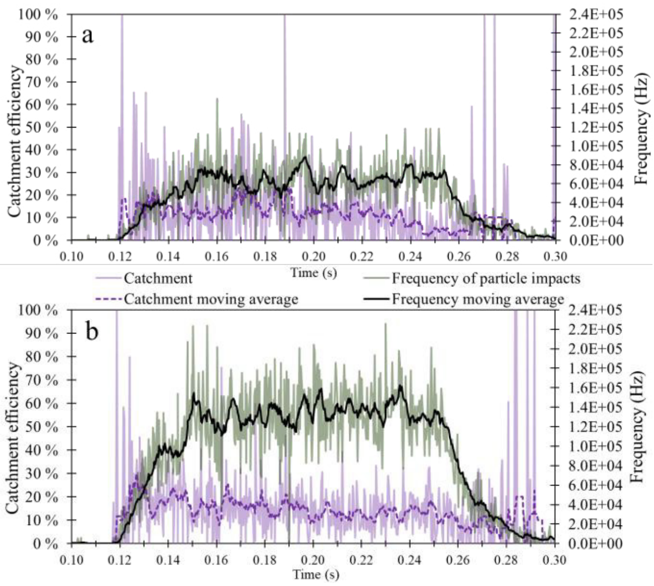

Fig. 7. Powder catchment efficiency and powder-substrate impact frequency of missing particles for (a) 5.21 g/min, (b) 11 g/min nozzle simulations.

Particles missing the melt pool impact the surrounding substrate and generate impact frequencies at 120-160 kHz at 11 g/min, with an average frequency of approximately 135 kHz during the steady powder flow period (0.16-0.25 s). For the lower mass flow rate (5.21 g/min), the particle impact frequency decreases to the 60-80 kHz bandwidth, consistent with the reduced particle flux. The lower particle density also increased the sensitivity of the impact frequency to catchment efficiency, revealing inverse correlations between catchment and particle impact frequency, e.g. at 0.18-0.22 s.

Using different lengths of moving average was observed to reveal or hide different instances of the mentioned inverse as well as positive correlations, which occur if the total powder mass flow rate changes. The impact frequency is therefore clearly linked to process variables such as mass flow rate and catchment efficiency; however, more simulation data and refined analysis techniques are needed to define these relationships. Nevertheless, the results indicate that detection of particle impact frequency has significant potential for monitoring crucial process variables such as catchment and mass flow rate.

The simulations further indicate that particles of different sizes interact differently with the gas flow and thus the melt pool. As shown in Fig. 8, certain particle diameters show a higher probability of reaching the melt pool, while others more frequently impact the substrate. Consequently, the size distribution of particles interacting with the melt pool differs from the nominal particle size distribution of the powder feedstock, suggesting that the particle impact frequency is influenced not only by the mass flow rate but also by the particle size distribution reaching the melt pool. Therefore, numerical simulation provides a useful tool for estimating the expected frequency range of particle impacts when interpreting acoustic emission data for different powder feedstocks.

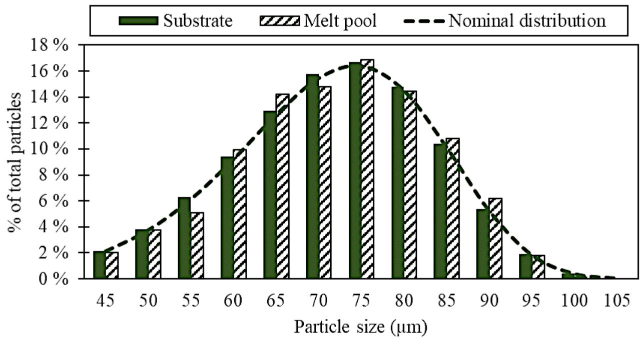

Fig. 8. Distribution of particles sizes which hit and miss the melt pool in the nozzle simulation compared to the nominal size distribution.

Figure 9 shows a typical FFT spectrum of the AE data obtained during bead deposition at the mass flow rate of 5.21 g/min. The experimental AE spectrum exhibits feature consistent with the theoretical thickness-resonance model, suggesting that powder impingement acts as a continuous, broadband acoustic exciter.

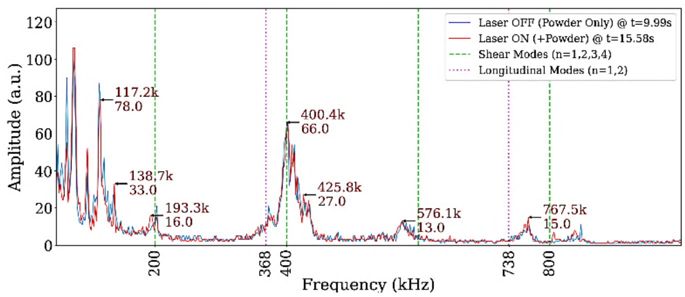

Fig. 9. FFT spectrum of AE signature from bead deposition at 1.4 kW laser power, 16 mm/s scan speed, and 5.21 g/min mass flow rate.

The frequency domain reveals amplitude peaks that generally align with the calculated harmonic frequencies: specifically, the observed shear modes near 200, 400, 600, and 800 kHz, and the longitudinal modes around 369 and 738 kHz. Although the fundamental frequency of the Rayleigh waves is estimated to exceed 7 MHz, it is excluded from our mapping because such extreme frequencies undergo severe material attenuation and fall beyond the sub-MHz limits of the employed sensor.

Notably, when comparing the powder-only state (laser OFF) to the active deposition state (laser ON), the fundamental structural resonance peaks remain relatively stable near their predicted locations. This observation is probably due to the low powder catchment rate which is about 22 % and it means 78 % of powders is still hitting the solid substrate and generate AE.

Peaks in AE data at roughly 30-50 kHz could correspond to the simulated impact frequency of 60-80 kHz, considering that the simulation is under-estimating the catchment efficiency, thus over-estimating the number of particles impacting the substrate, by 40 %. Further study in different process conditions is required to confirm this connection. Despite this limitation, the simulations provide realistic estimates of particle impact frequencies, which form the basis for interpreting the AE signals measured during the experiments.

Conclusion

The simulated particle impact frequencies provide an estimate of the acoustic excitation generated by powder-substrate interactions during the DED-LB process. The results establish a physical basis for interpreting the experimentally measured acoustic emission signals, enabling correlation between AE spectral features and variations in powder mass flow rate and catchment efficiency.

The primary outputs of the melt pool simulation are the melt pool geometry used as input for the nozzle simulation, and the resulting bead width, which serves as the validation parameter. The DED-LB nozzle was simulated using a coupled CFD-DEM model, key results including the frequency of particle impacts on the substrate as well as the time-resolved catchment efficiency, which is also used for validation. These results reveal notable correlations, suggesting that acoustic emission monitoring may be a suitable approach for real-time observation of catchment efficiency and mass flow rate.

Spectral analysis of the experimental structure-borne AE signals indicates that powder impingement acts as a continuous broadband acoustic source, exciting stable structural resonances that are largely independent of laser dynamics. The observed shear and longitudinal bulk modes show good agreement with the calculated substrate harmonics. Supported by CFD modelling, these AE signals demonstrate high sensitivity to variations in powder mass flow rate, enabling reliable detection of flow fluctuations.

Although AE successfully tracks these mass flow dynamics, the direct quantification of absolute powder catchment efficiency from acoustic measurements alone remains challenging. This study demonstrates that integrating AE monitoring with computational modeling provides a highly promising pathway for the real-time evaluation of powder delivery efficiency and overall process stability in DED-LB.

To refine the quantitative link between AE and catchment efficiency and enhance efficiency and predictability of the DED-LB process, further studies are required. For example, to utilize ultra-wideband transducers to include the high-frequency Rayleigh signatures, while also investigating deposition with higher catchment efficiency to isolate pure melt pool AE. To refine the CFD model for use in wider process regimes, parameter-dependent initial conditions and validation and testing in various process conditions are needed.

Acknowledgements

The authors acknowledge the support from the Department of Mechanical and Materials Engineering at the University of Turku, and Quad Tech Turku, Turku, Finland. This study used FLOW-3D AM® (Version 2025R1U1; Flow Science, Inc.) made available through the FLOW-3D Academic Program.

References

[1] Mahamood RM. Areas of application of laser metal deposition process - part repair and remanufacturing. In: Laser metal deposition process. 2018. p. 143-164. doi:10.1007/978-3-319-64985-6_7.

[2] Saboori A, Aversa A, Marchese G, Biamino S, Lombardi M, Fino P. Application of directed energy deposition-based additive manufacturing in repair. Appl Sci 2019; 9(16):3316. doi:10.3390/app9163316.

[3] Ahn DG. Directed energy deposition (DED) process: state of the art. Int J Precis Eng Manuf-Green Technol 2021;8(2):703-742. doi:10.1007/s40684-020-00302-7.

[4] Lalegani Dezaki M, et al. A review on additive/subtractive hybrid manufacturing of directed energy deposition (DED) process. Adv Powder Mater 2022; 1(4):100054. doi:10.1016/j.apmate.2022.100054.

[5] Urresti A, Murua O, Arrizubieta JI, Lamikiz A. In-situ monitoring of the DED-LB process for defect detection. Procedia CIRP 2024;124:314-317. doi:10.1016/j.procir.2024.08.125.

[6] Zhou Y, Jiang D, Al-Akailah A, Ning F. Understanding the formation of laser-induced melt pools with both wire and powder feedstock. Addit Manuf 2024; 89:104312. doi:10.1016/j.addma.2024.104312.

[7] Kumar P, Jain NK, Dixit P. Modelling of powder catchment efficiency in micro-plasma transferred arc metal additive manufacturing process. Prog Addit Manuf 2025; 10(4):2161-2175. doi:10.1007/s40964-024-00742-6.

[8] Tang ZJ, et al. A review on in situ monitoring technology for directed energy deposition of metals. Int J Adv Manuf Technol. doi:10.1007/s00170-020-05569-3.

[9] Liu H, et al. Numerical simulation of powder transport behavior in laser cladding with coaxial powder feeding. Sci China Phys Mech Astron 2015; 58(10):104701. doi:10.1007/s11433-015-5705-4.

[10] Saldi Z, Pasang T, Khogres W, Budiman A, Gunawan F. Numerical simulations of fluid flows and heat transfer in melt pools of directed energy deposition of SS316L. E3S Web Conf 2024; 484:03010. doi:10.1051/e3sconf/202448403010.

[11] Whiting J, Springer A, Sciammarella F. Real-time acoustic emission monitoring of powder mass flow rate for directed energy deposition. Addit Manuf 2018; 23:312-318. doi:10.1016/j.addma.2018.08.015.

[12] Kouprianoff D, Yadroitsava I, du Plessis A, Luwes N, Yadroitsev I. Monitoring of laser powder bed fusion by acoustic emission: investigation of single tracks and layers. Front Mech Eng 2021; 7. doi:10.3389/fmech.2021.678076.

[13] Ursprung M, Heine T, Fischer B, Wolfgang R, Sommerhuber R. Monitoring additive manufacturing with an optical microphone. Vienna; 2019.

[14] Boschetto A, Quadrini F. Powder size measurement by acoustic emission. Measurement 2011; 44(1):290-297. doi:10.1016/j.measurement.2010.10.005.

[15] Buttle DJ, Scruby CB. Characterization of particle impact by quantitative acoustic emission. Wear 1990; 137(1):63-90. doi:10.1016/0043-1648(90)90018-6.

[16] Heinlein S, Mariani S, Milewczyk J, Vogt T, Cawley P. Improved thickness measurement on rough surfaces by using guided wave cut-off frequency. NDT E Int 2022; 132:102713. doi:10.1016/j.ndteint.2022.102713.d